

Neural Distributed Source Coding

Jay Whang

jaywhang@cs.utexas.edu
University of Texas at Austin

Anish Acharya

anishacharya@utexas.edu
University of Texas at Austin

Hyeji Kim

hyeji.kim@austin.utexas.edu
University of Texas at Austin

Alexandros G. Dimakis

dimakis@austin.utexas.edu
University of Texas at Austin

May 25, 2022

Abstract

Distributed source coding (DSC) is the task of encoding an input in the absence of correlated side information that is only available to the decoder. Remarkably, Slepian and Wolf showed in 1973 that an encoder without access to the side information can asymptotically achieve the same compression rate as when the side information is available to it. While there is vast prior work on this topic, practical DSC has been limited to synthetic datasets and specific correlation structures. Here we present a framework for lossy DSC that is agnostic to the correlation structure and can scale to high dimensions. Rather than relying on hand-crafted source-modeling, our method utilizes a conditional VQ-VAE to learn the distributed encoder and decoder. We evaluate our method on multiple datasets and show that our method can handle complex correlations – significantly better than the current state-of-the-art method.

1 Introduction

Data compression plays an essential role in modern computer systems. From multimedia codecs running on consumer devices to cloud backups in large data centers, compression is a necessary component in any system that deals with high-volume or high-velocity sources. Applications such as multi-camera surveillance systems, IoT sensing, 3D scene capture and stereo imaging create distributed data streams with very large volume that are highly correlated.

We are interested in distributed compression – specifically the *distributed source coding* problem. In this setting, there are two correlated sources (input x and side information y) that are physically separated. Both must be compressed and sent to a common decoder. We can assume that the side information y is compressed in isolation and communicated to the decoder and now one can expect that the original source x can be compressed at a higher-rate since y is known to the decoder.

The core challenge is how to compress the original source x when the correlated side information y is available only at the decoder as shown in fig. 1 (left). If side information is available to both the encoder and decoder as in fig. 1 (right), it is well known that the side information can be utilized to improve the compression rate of x .

Surprisingly, in 1973, Slepian and Wolf [1] showed that an encoder that has no access to the correlated side information can asymptotically achieve the same compression rate as when side information is available at both the encoder and the decoder. In other words, *distributed* compression

is asymptotically as efficient as *joint* compression. Later, Wyner and Ziv [2] extended this result to lossy compression. This is nothing short of a remarkable classical information theory result that defies intuition.

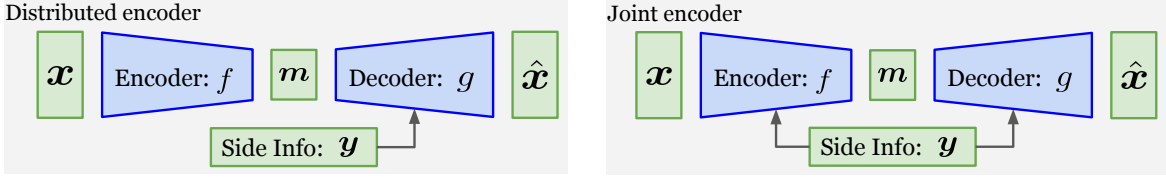


Figure 1: A distributed encoder that has no access to the correlated side-information (left) can asymptotically achieve the same compression rate as when side-information is available at both the encoder and the decoder (right).

1.1 Motivating Example

To provide some intuition behind distributed source coding, we describe a simple example that illustrates how side information known *only* to the decoder can be as useful as side information known to *both* the encoder and decoder [3].

Let x and y be the two correlated sources, here uniformly random 3-bit sources, which differ by at most one bit (i.e., Hamming distance between x and y is at most one). Clearly, to losslessly compress x without any side information, the encoder has to send 3 bits to the decoder. If y is known to both the encoder and decoder, then x can be transmitted using only 2 bits instead, since the encoder can send the difference between x and y , which is uniform in $\{000, 100, 010, 001\}$. Therefore *joint* compression using only 2 bits is possible.

Now, if the side information y is available only at the decoder, Slepian-Wolf theorem suggests that the encoder can still transmit x using only 2 bits. How could this be possible? The key idea is to group 8 possible values of x into 4 bins, each containing two bit-strings with maximal Hamming distance: $\mathcal{B}_0 = \{000, 111\}$, $\mathcal{B}_1 = \{001, 110\}$, $\mathcal{B}_2 = \{010, 101\}$, $\mathcal{B}_3 = \{011, 100\}$. Then the encoder simply transmits the bin index $m \in \{0, 1, 2, 3\}$ for the bin containing x . The decoder can produce the reconstruction \hat{x} based on the bin index m and y ; precisely, $\hat{x} = \arg \max_{x \in \mathcal{B}_m} P(x|y)$. In this case, since the Hamming distance between x and y is at most one and the Hamming distance between the bit strings in each bin is 3, the decoder can recover x without error. The side information allows the decoder to correctly choose between the two candidates in the bin specified by the encoder.

1.2 Practical Difficulties

There are major challenges in designing practical distributed compression schemes for arbitrarily correlated sources. First, the joint distribution $p(x, y)$ is required to design the encoder and decoder, but modeling high-dimensional joint distributions (e.g. for correlated images) is very challenging, especially without modern deep generative models. Second, designing a distributed compression scheme with reasonable run time beyond simple structures remains an open question.

The significant gap between the theory of Slepian-Wolf and Wyner-Ziv and what is efficiently achieved in practice has been well-acknowledged in the information theory community. Two decades after the Slepian-Wolf theorem, Verdu [4] writes: “despite the existence of potential applications, the conceptual importance of Slepian–Wolf coding has not been mirrored in practical data compression.” Constructive compression schemes have been designed only for very special cases, such as correlated Gaussian sources [3] and stereo images (as elaborated in Section 2.3).

In this paper, we bridge this gap by leveraging the recent advances in deep generative modeling and show that it is possible to train an encoder and decoder for distributed compression of *arbitrarily*

correlated high-dimensional sources. Specifically, our approach (denoted *Neural DSC*) parametrizes the encoder-decoder pair as a Vector-Quantized VAE (VQ-VAE) [5], so that: (a) we do not need a hand-crafted analytical model for the joint distribution; and (b) we can *learn* the complicated encoder and decoder mappings via neural networks and execute them efficiently at inference time; and (c) the discrete latent representation of VQ-VAE provides a *data-driven* quantization scheme that avoids the need for manual quantization and entropy coding to obtain the compressed message.

Our main contributions are as follows:

- We introduce Neural DSC, a compression scheme for lossy distributed source coding based on VQ-VAE. Our encoder without side information creates the compressed message, which is then transmitted to the decoder that reconstructs the original signal by leveraging the side information.
- We show that Neural DSC performs favorably to existing techniques on stereo camera image compression. Specifically, it outperforms existing methods for low rates and remains competitive at high rates.
- We further validate that our approach can adapt to complex correlations. For this, we compress the top half of an image given the bottom part as side information. On this task, our method significantly outperforms the current state-of-the-art method and nearly matches the joint compression rate.
- We provide a promising evidence that Neural DSC is effective in other modalities by applying it to gradient compression for distributed model training.
- We compare our model to the theoretical optimum on synthetic data and provide evidence that our model indeed learns to perform distributed source coding. We also show that learned quantization scheme is critical to the model’s performance.

2 Neural Distributed Source Coding

2.1 Vector-Quantized VAE

Vector-Quantized VAE (VQ-VAE) [5] is a specific type of VAE [6, 7] that has a *discrete* latent variable, even though the input is continuous. Because the latent code is discrete and has fixed size, VQ-VAEs are a natural fit for lossy compression. Indeed, many existing works have explored its use in various compression tasks, ranging from music generation to high-resolution image synthesis [8–10]. Most recently, a variant of VQ-VAE was used to generate discrete embedding for natural images for zero-shot text-to-image generation [11].

A VQ-VAE consists of three components: an encoder, a decoder, and a codebook. The main difference between VQ-VAE and a regular VAE is that the output of the encoder is quantized to the nearest vector in the codebook. During training, all three components are jointly optimized. The fact that VQ-VAE learns the quantization scheme from data is important, as we further explain in section 4. During inference, the input is represented by the index of the codebook vector that the encoder’s output is quantized to.

2.2 Our Method

Notation and Setup. We let x , y , and m to denote the input signal, correlated side information, and compressed message, respectively. The encoder f generates the compressed message: $m = f(x)$; the decoder g creates the reconstruction \hat{x} with the aid of the side information: $\hat{x} = g(m; y)$. Note that the encoder only receives x , while the decoder receives both the compressed message m and the side information y . We refer to the number of bits required to transmit m as the *rate*, and the

reconstruction performance (e.g. measured by ℓ_2 error) as the *distortion*. In general, higher rate leads to lower distortion, and vice versa.

We propose to learn the distributed encoder f and decoder g for (\mathbf{x}, \mathbf{y}) by parametrizing f and g as a conditional VQ-VAE, where g is conditioned on the side information \mathbf{y} . The network is trained on i.i.d. pairs $\{(\mathbf{x}^{(i)}, \mathbf{y}^{(i)})\} \sim p(\mathbf{x}, \mathbf{y})$ to minimize the ℓ_2 distortion between the input \mathbf{x} and the reconstruction $\hat{\mathbf{x}}$. This scheme allows us to directly train the encoder-decoder pair in an end-to-end manner without needing to model or manually specify the correlation structure between \mathbf{x} and \mathbf{y} .

Why VQ-VAE? Although much of the existing literature has focused on VAEs as the backbone for neural compression [12–16], we intentionally chose VQ-VAE instead for a few reasons. First, VQ-VAE offers an explicit control over the rate through the latent dimension and codebook size – unlike VAEs for which we can only estimate the rate after training the model. VQ-VAE also guarantees an upper bound on the resulting rate regardless of the input, which is often desired in practice (e.g. communication channel with strict bandwidth limit). The downside of using a VQ-VAE is that training is less stable than a VAE, but this did not pose much issue during our experiments.

2.3 Related Work

Unlike the vast literature that exists on distributed source coding (DSC), the use of deep learning on DSC has received relatively little attention. To the best of our knowledge, we are aware of two relevant studies, which we describe below.

Distributed Stereo Image Compression [17] proposes a method to perform DSC for stereo camera image pairs with a high spatial correlation. Due to the large spatial similarity between the images, one of them can serve as the side information for the other. The key component of their method is the “Side Information Finder”, a module that finds similar image patches between the side information and the reconstructed signal produced by a pre-trained autoencoder. Since the two images have many approximately overlapping patches, the reconstruction is further improved by copying over matching image patches from the side information to the reconstruction.

While this leads to a considerable improvement in compression performance, this method is only applicable when the input and side information have large spatial overlap. On the other hand, our method is applicable to any correlated sources. We empirically validate this using data sources with substantially more complex correlation (see Figure 2b).

Neural Distributed Image Compression [18] is the most recent and current state-of-the-art method that leverages a (regular) VAE for DSC of image data. The proposed architecture is designed to explicitly model the common information between the input and side information. Intuitively, the goal is to guide the encoder to compress only the portion that is not recoverable from the side information. Once trained, the encoder simply discards the common information and only transmits the residual, with the hope of decoder being able to reconstruct the common information from the side information. As [18] is closely related to our work and is the current state-of-the-art method that improves upon [17], we compare our method with both of these methods in our experiments.

3 Experiments

3.1 Stereo Image Compression

Setup. We first evaluate our method on stereo image compression. Following [17], we construct a dataset consisting of pairs of images obtained from the KITTI Stereo 2012 and 2015 [19, 20]. Each pair of images are taken by two cameras at a slightly different angle and share spatial similarity (see fig. 2b, left). The goal is to compress one of the images in each pair, treating the other image as side information that only the decoder has access to. The performance of a compressor is evaluated by its

rate-distortion points, where rate and distortion are measured in terms of bits/pixel (bpp) and Peak Signal-to-Noise Ratio (PSNR). To the best of our knowledge, this is the only benchmark that currently exists for distributed image compression.

For each target rate, we train a conditional VQ-VAE as described in section 2.2. We then evaluate its distortion averaged over the test set, and plot the rate-distortion point. The exact details of how the dataset is constructed as well as the model hyperparameters are included in the Appendix.

Results. We compare our methods to existing distributed image compression methods DSIN [17] and NDIC [18]. As shown in fig. 2a, our method achieves new state-of-the-art distortion for rates below 0.25 bits/pixel. For higher rate, our method is slightly worse compared to NDIC.

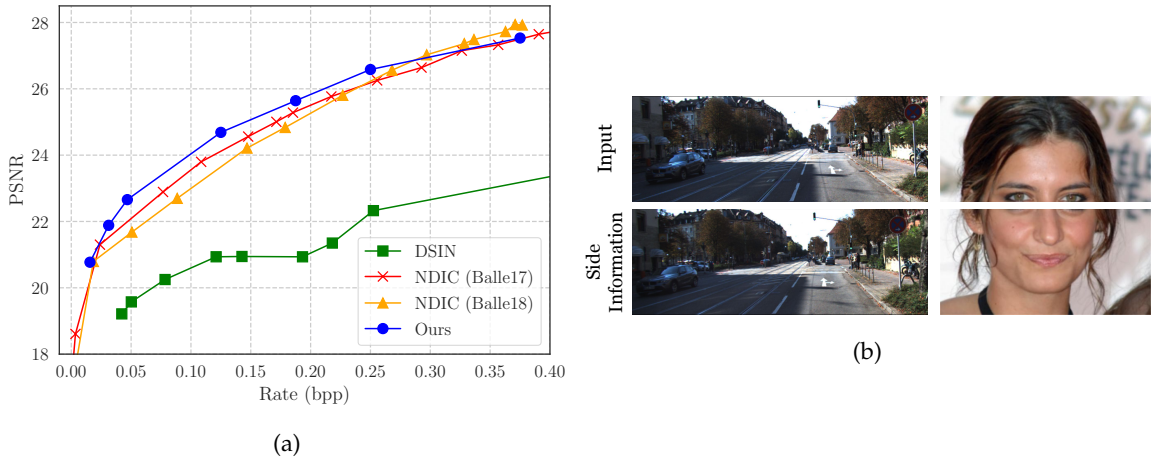


Figure 2: **Left:** Comparison of rate-distortion curves on the KITTI Stereo image dataset. Our method achieves higher PSNR than other methods for low rates and remains competitive for higher rates. **Right:** Sample image pairs from our distributed image compression experiments. Compared to the KITTI Stereo pairs, the CelebA-HQ [21] pairs exhibit far more complex correlations.

In addition, our model is significantly more parameter-efficient compared to [18]. Table 1 shows the parameter count for the models used to generate the points in fig. 2a. As shown, our models are smaller by a factor of up to $\sim 6\times$.

Table 1: Number of model parameters for the rate-distortion points in fig. 2a. We see that our models are much more parameter-efficient while achieving competitive rate-distortion. The last column shows relative size compared to the smallest model we used.

	Parameter Count (M)	Factor
Ours	4.0 – 6.3	1.0-1.6 \times
NDIC (Ballé17)	16.3	4.1 \times
NDIC (Ballé18)	25.0	6.25 \times

3.2 Handling Complex Correlation

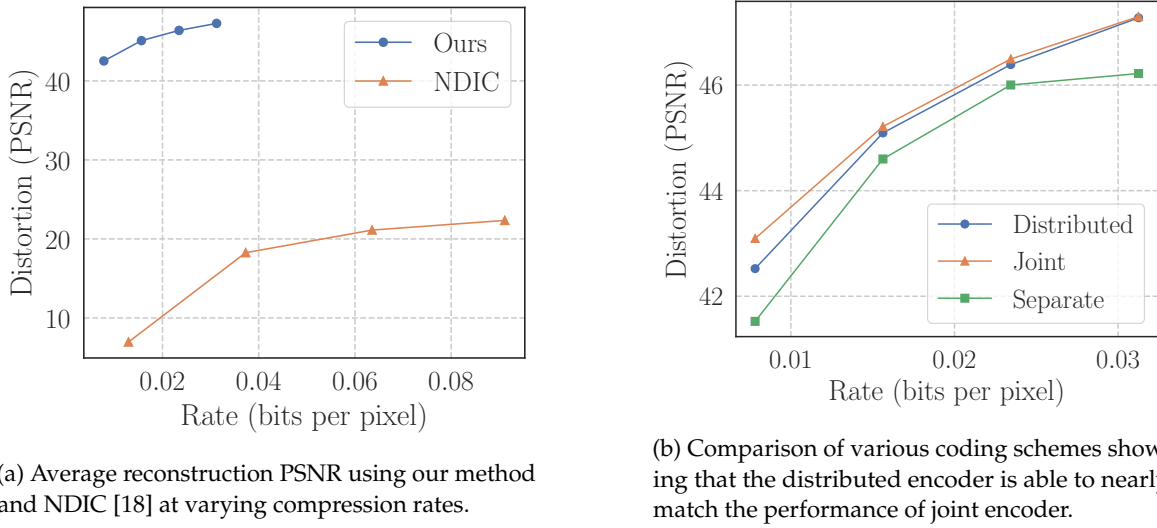
Setup. To further investigate how well our method can handle complex correlation between the input and side information, we evaluate our method on a challenging distributed compression setup. First we create a dataset of correlated images from 256×256 CelebA-HQ dataset [21] containing images of celebrity faces. Each image is vertically split into top and bottom halves, where the top half is used as

the input and the bottom half is used as side information. Following [22], we use 27000/3000 split between training and test data.

While there is clearly some correlation between the top and bottom halves of an image of a human face, modeling this correlation (e.g. the conditional distribution over the top half of a face given the bottom half) is highly nontrivial. This experiment is thus designed to show our model’s ability to leverage this correlation to improve compression performance.

Baseline VQ-VAEs. To analyze the gains from distributed compression, we train three different variants of VQ-VAEs: distributed (our method), joint, and separate. In the *joint* model, both the encoder and decoder have access to the side information. This serves as a proxy to the intractable theoretical rate-distortion bound established by Wyner and Ziv [2] for lossy distributed compression. We expect this to be the upper limit on the performance of our method. The *separate* model is positioned at the other extreme, where neither the encoder nor the decoder uses the side information. This serves as the lower limit on the performance of our method. To ensure a fair comparison among these variants, they have identical architecture and number of parameters for the autoencoder portion, and only vary in the way they handle the side information. Architectural details and network hyperparameters are provided in the Appendix.

Results. In Figure 3, we present rate-distortion curves for our model as well as NDIC evaluated over the test set. We adopt the commonly used distortion metric Peak Signal-to-Noise Ratio (PSNR). Figure 3a shows that our method achieves a significantly better rate-distortion performance compared to NDIC [18] in the presence of complex correlation between the image pair. We posit that this is due to NDIC attempting to explicitly model the correlation even though it is not used during inference. In Figure 3b, we see that the distributed VQ-VAE achieves nearly identical performance as the joint VQ-VAE, further proving the viability of our method as a distributed coding scheme.



(a) Average reconstruction PSNR using our method and NDIC [18] at varying compression rates.

(b) Comparison of various coding schemes showing that the distributed encoder is able to nearly match the performance of joint encoder.

Figure 3: Rate-distortion curves for distributed compression of images with complex correlation.

Effect of Side Information. It is possible that the distributed VQ-VAE learns to ignore the side information, effectively collapsing to a separate VQ-VAE. We investigate whether the distributed decoder actually makes use of the side information by intentionally providing incorrect input.

We can see in Figure 4 that the side information plays a significant role in the quality of reconstruction. For example, providing a side information with a different face leads to the reconstruction

having a matching skin tone that is different from the original. As expected, side information has no effect for the separate encoder.



Figure 4: Reconstructions from distributed encoder under different side information. We can see that providing wrong or random side information to the distributed decoder affects the output in a semantic way (e.g. the skin tone changes, while the background remains identical).

3.3 Communication Constrained Distributed Optimization

Background. Here we consider an interesting application of our method to distributed training of a neural network h_θ with parameters $\theta \in \mathbb{R}^d$. Mini-batch SGD and other first order methods such as Adam [23] have become the de-facto standard for optimizing such functions [24–26]. With the increasing size of deep learning models, it is necessary to train a model across multiple workers¹. In particular, each worker j is assigned a subset $\mathcal{X}_j \in \mathcal{X}$ of the training data. The workers then compute gradients locally using SGD-like iterations and communicate the gradients back to a central parameter server. The server then aggregates the received gradients to perform a global update and broadcasts the updated parameters back to the workers.

An important bottleneck in this setting is the repeated communication of gradients between workers and the server, often resulting in significant communication overhead, especially for large models. To alleviate this issue, many gradient compression techniques have been developed. Here we present a promising proof of concept that demonstrates that our distributed encoder is able to better compress gradients compared to several established techniques.

Experimental Setup. We focus on a simple setting with two workers interacting with a central server. The key observation is that, at each iteration t , the correlation between the client gradients \mathbf{g}_t^1 and \mathbf{g}_t^2 can be exploited to further improve compression performance by viewing this as a distributed compression task. Concretely, we treat \mathbf{g}_t^1 as side information and train a distributed encoder for \mathbf{g}_t^2 , and show that the cost of communicating \mathbf{g}_t^2 can be substantially reduced.

The neural network h_θ being trained using compressed gradients is a small convolutional network for MNIST [27] digit classification. We partition the MNIST training data \mathcal{X} into two equal subsets: \mathcal{X}_{pre} and \mathcal{X}_{train} . \mathcal{X}_{pre} is used to train the VQ-VAE encoder and \mathcal{X}_{train} is used to train h_θ using the trained encoder as gradient compressor. We measure the performance of our method using two metrics: (a) **rate-distortion** of the distributed compressor, and (b) **classification accuracy** of the model h_θ trained using compressed gradients.

Generating training data for encoder. We train h_θ for T steps using the Adam optimizer across two nodes over \mathcal{X}_{pre} . This generates a sequence of T gradient pairs $\{\mathbf{g}_t^1, \mathbf{g}_t^2\}_{t=1}^T$, which can be used to train the VQ-VAE encoders.

However, naively applying our method to this setting leads to a suboptimal VQ-VAE as these gradient pairs are highly correlated. Noticing that \mathbf{g}_t^1 and \mathbf{g}_t^2 are conditionally independent given the

¹We use the terms node, client and worker interchangeably.

initial model weights and the time step t , we train h_θ for multiple runs with different initialization for θ , while randomly sampling a subset of gradients from each run. Thus we generate a dataset of tuples $(t, \mathbf{g}_t^1, \mathbf{g}_t^2)$ sampled from multiple independent runs. We also update the architecture of the VQ-VAE so that both the encoder and decoder are conditioned on t . This way, the gradients become i.i.d. samples over random runs and time steps. We consider the following baseline methods for our comparison:

- **Random- k** [28, 29]: Instead of communicating the full gradient vector $\mathbf{g} \in \mathbb{R}^d$, we only transmit randomly chosen k coordinates, thus reducing the communication cost by a factor of $\frac{k}{d}$.
- **Top- k** [30, 31]: Similar to Random- k , this approach also communicates k of the d coordinates of a gradient vector and improves the communication cost by a factor of $\frac{k}{d}$. However, this time we take the top k coordinates with largest magnitude and discard the remaining $(d - k)$ coordinates.
- **QSGD** [32, 33]: Gradients normally stored using 32-bit floating point numbers are quantized using fewer bits before being transmitted.
- **Coordinated Sampling** [34]: The nodes *cyclically* select a batch of k coordinates at every iteration and communicate only those k coordinates.

Pre-training VQ-VAE encoders. We first compare the performance of three different VQ-VAE variants over the course of a single training run of h_θ . As shown in Figure 5a, we observe a substantial improvement in ℓ_2 distortion for the distributed VQ-VAE, compared to the separate model. As training progresses, the gap between the joint and distributed encoders narrows, suggesting that a sufficiently large distributed VQ-VAE encoder can nearly match the performance of its joint counterpart.

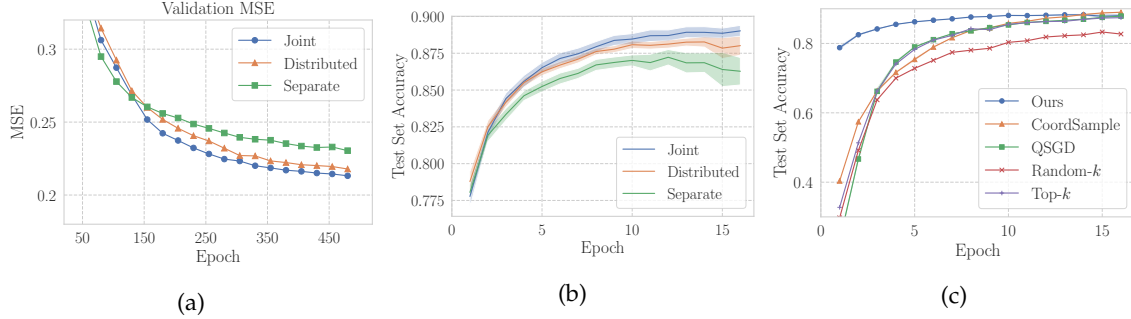


Figure 5: **Left:** Average ℓ_2 distortion over the validation split during the course of VQ-VAE training. We observe that the distributed encoder significantly outperforms the separate encoder and approaches the distortion of the joint encoder.

Center: Plot of the average test set accuracy over the course of training h_θ using compressed gradients. We observe that the distributed encoder leads to comparable accuracy as the joint encoder, but using about only half of the communication cost. Shaded regions represent standard error. **Right:** Distributed training performance with compressed gradients using a distributed encoder in comparison to other baseline methods in terms of test set accuracy. Note that standard error is very small and barely visible, and may require zooming in on an electronic copy of this manuscript.

Distributed Training. Given the pre-trained encoders, we train h_θ using gradients compressed by the pre-trained encoder. We compare it against the baseline gradient compression schemes listed above: Top- k , Rand- k , QSGD and Coordinated Sampling. All runs were repeated 20 times with different random seeds, and we report average performance along with standard error.

Figure 5b shows that h_θ trained with gradients compressed using the distributed VQ-VAE leads to substantial accuracy improvement over the separate VQ-VAE without the extra communication

cost. Moreover, we see that VQ-VAE based compression leads to about $3\times$ faster convergence than the baselines (see fig. 5c). This shows that a learned distributed encoder can indeed benefit from the complex correlation between gradients distributed optimization.

4 Discussion and Analysis

Role of Side Information. In Section 1.1 we saw that grouping symbols with maximal distance from each other in the same group allows the decoder to determine the correct symbol using the side information. Here we investigate to what extent our models perform such a grouping (also known as *binning*). If approximate binning was occurring, the same codeword (i.e. bin index) would be decoded into different images for different side information. In other words, a distributed compressor should have high reconstruction diversity for a single codeword as we vary the side information. We refer to this as *bin diversity*.

On the other hand, a model that does not perform binning should decode a single codeword to similar symbols regardless of what side information is given to the decoder. To test this hypothesis, we train two different models: **Ours** – trained with the correct side information as was done for other experiments; **Uncorrelated SI** – trained by replacing the side information with random ones from other, irrelevant samples in the dataset, thus making the input and side information completely independent. We expect this model to ignore side information and achieve lower bin diversity.

To quantitatively measure diversity, we used average pairwise distance with respect to ℓ_2 norm and LPIPS distance [35], which has been used in the literature [36, 37] as a measure of sample diversity. Both metrics were computed and averaged over all images in the CelebA-HQ test dataset.

As shown in table 2, the VQ-VAE trained with correlated side information exhibits much higher bin diversity in both metrics. In other words, the images within each bin are much farther from each other compared to the other model, suggesting that some form of approximate binning is happening. The uncorrelated VQ-VAE has particularly low bin diversity with respect to the LPIPS distance, meaning there is very little perceptual difference regardless of what side information is used.

Table 2: Diversity of decoded samples as we vary side information. Notice that our model produces diverse samples, whereas the baseline (Uncorrelated SI) achieves very low bin diversity. This suggests that our model performs binning correctly and learns to utilize the side information.

	Diversity (LPIPS)	Diversity (ℓ_2)
Ours	0.1130	35.80
Uncorrelated SI	0.00469	4.167

Optimality of the Learned Compressor. Another natural question to ask is how close our *learned* distributed compressor is to the optimal distributed compressor. We investigate this using a synthetic data source studied in [3] with two correlated Gaussian sources: $Y = X + N$, $X \sim \mathcal{N}(0, 1)$, and $N \sim \mathcal{N}(0, 0.1^2)$. The asymptotically optimal (i.e. in the limit of compressing infinitely many symbols together) rate-distortion curve of these sources is known analytically, so we can check how our model compares to the theoretical limit.

Figure 6a shows that for low rates, both learned methods significantly outperform the asymptotically optimal encoder without side information (SI). This is a concrete evidence that our learned encoder is actually performing DSC (as opposed to simply achieving a very good compression rate for single source coding) Moreover, the distributed compression performance remains very close to that of joint compression, showing the efficacy of our practical distributed coding scheme.

At higher rates, however, the value of side information quickly diminishes, and the learned methods perform worse than even the encoder without SI. This is expected as the optimal curves presented in this figure are asymptotic in the limit of jointly compressing infinitely many symbols, which is clearly not the case for the learned methods that compress each symbol one at a time.

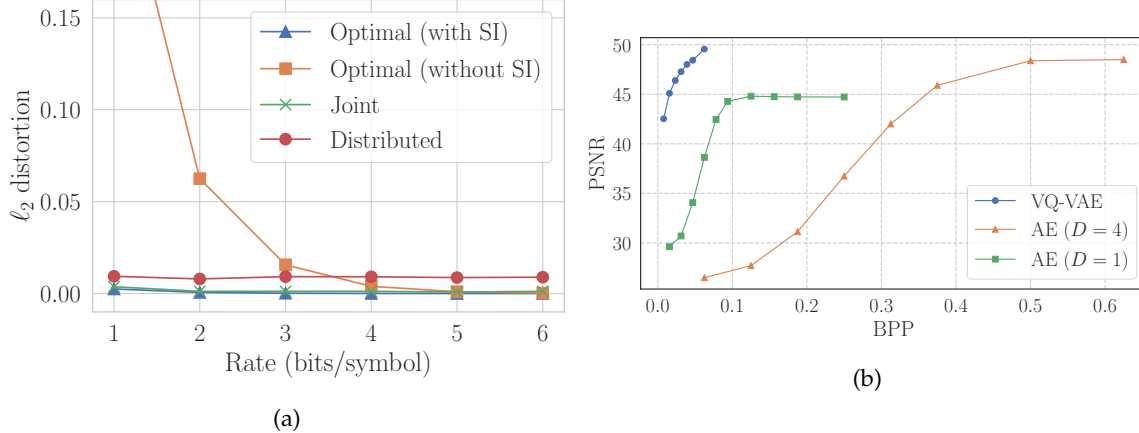


Figure 6: **Left:** Rate-distortion points of learned joint and distributed encoders compared to theoretically best compressors. The “Optimal” curves represent the asymptotically optimal rate-distortion points and are included as reference. Note that these are theoretical limits and do not correspond to any concrete compression scheme.

Right: Ablation for the importance of *learned* vector quantization. We see that identical encoder/decoder architecture *without* the learned quantization scheme performs far worse than the the one with a learned quantization scheme.

Importance of Learned Quantization. As mentioned in section 2.1, we test the importance of *learned* quantization of VQ-VAE, which likely contributes to the performance gains compared to NDIC given that NDIC uses uniform quantization. We do so by plotting the rate-distortion curve of an autoencoder with identical network architecture as our VQ-VAE models, but with uniform quantization.

Once trained, the continuous latent variables are uniformly quantized to different levels, thus producing multiple rate-distortion points as shown in Figure 6b. We see that VQ-VAE enjoys a significantly improved performance due to the data-driven quantization scheme. Even when we increase the latent dimension ($D = 1$ vs $D = 4$) for the autoencoder with uniform quantization, the resulting distortion is still worse than VQ-VAE, even at a significant cost of compression rate.

That said, a more sophisticated quantization scheme tailored to the downstream task may lead to substantial improvements. Studying better quantization schemes or even quantization-less compression techniques is an active area of research [38, 39], which we leave for future work.

5 Conclusions

We presented Neural DSC, a framework for distributed compression of correlated sources. Our method is built on the power of modern deep generative models, namely VQ-VAEs, which are excellent data-driven models to represent high-dimensional distributions using compressed discrete latent codes. For stereo image compression, our method performs better or competitively compared to existing techniques. We also show that our method is able to leverage complex correlations far beyond spatial similarity for better compression performance, approaching the joint compression rate. Finally, we show that our method is not limited to images and show a promising result for compressing

gradients for distributed model training. We believe that our work provides encouraging initial results for practical data-driven distributed compression schemes and hope to see further developments.

Acknowledgments

This research has been supported by NSF Grants CCF 1934932, AF 1901292, 2008710, 2019844 the NSF IFML 2019844 award as well as research gifts by Western Digital, WNCG and MLL, computing resources from TACC and the Archie Straiton Fellowship.

References

- [1] D. Slepian and J. Wolf. Noiseless coding of correlated information sources. *IEEE Transactions on Information Theory*, 19(4):471–480, 1973. doi: 10.1109/TIT.1973.1055037.
- [2] A. Wyner and J. Ziv. The rate-distortion function for source coding with side information at the decoder. *IEEE Transactions on Information Theory*, 22(1):1–10, 1976. doi: 10.1109/TIT.1976.1055508.
- [3] S.S. Pradhan and K. Ramchandran. Distributed source coding using syndromes (discus): design and construction. In *Proceedings DCC’99 Data Compression Conference (Cat. No. PR00096)*, pages 158–167, 1999. doi: 10.1109/DCC.1999.755665.
- [4] S. Verdu. Fifty years of shannon theory. *IEEE Transactions on Information Theory*, 44(6):2057–2078, 1998. doi: 10.1109/18.720531.
- [5] Aaron van den Oord, Oriol Vinyals, and Koray Kavukcuoglu. Neural discrete representation learning. In *Proceedings of the 31st International Conference on Neural Information Processing Systems*, pages 6309–6318, 2017.
- [6] Diederik P. Kingma and Max Welling. Auto-encoding variational bayes. In Yoshua Bengio and Yann LeCun, editors, *2nd International Conference on Learning Representations, ICLR 2014, Banff, AB, Canada, April 14-16, 2014, Conference Track Proceedings*, 2014. URL <http://arxiv.org/abs/1312.6114>.
- [7] Danilo Jimenez Rezende, Shakir Mohamed, and Daan Wierstra. Stochastic backpropagation and approximate inference in deep generative models. In *International conference on machine learning*, pages 1278–1286. PMLR, 2014.
- [8] Cristina Garbacea, Aaron van den Oord, Yazhe Li, Felicia S C Lim, Alejandro Luebs, Oriol Vinyals, and Thomas C Walters. Low bit-rate speech coding with vq-vae and a wavenet decoder. *ICASSP 2019 - 2019 IEEE International Conference on Acoustics, Speech and Signal Processing (ICASSP)*, May 2019. doi: 10.1109/icassp.2019.8683277. URL <http://dx.doi.org/10.1109/ICASSP.2019.8683277>.
- [9] Ali Razavi, Aaron van den Oord, and Oriol Vinyals. Generating diverse high-fidelity images with vq-vae-2. In H. Wallach, H. Larochelle, A. Beygelzimer, F. d’Alché-Buc, E. Fox, and R. Garnett, editors, *Advances in Neural Information Processing Systems*, volume 32. Curran Associates, Inc., 2019. URL <https://proceedings.neurips.cc/paper/2019/file/5f8e2fa1718d1bbcadf1cd9c7a54fb8c-Paper.pdf>.
- [10] Adam Roberts, Jesse Engel, Colin Raffel, Curtis Hawthorne, and Douglas Eck. A hierarchical latent vector model for learning long-term structure in music. In *International Conference on Machine Learning*, pages 4364–4373. PMLR, 2018.

- [11] Aditya Ramesh, Mikhail Pavlov, Gabriel Goh, Scott Gray, Chelsea Voss, Alec Radford, Mark Chen, and Ilya Sutskever. Zero-shot text-to-image generation. *arXiv preprint arXiv:2102.12092*, 2021.
- [12] Johannes Ballé, Valero Laparra, and Eero P. Simoncelli. End-to-end optimized image compression, 2017.
- [13] Lucas Theis, Wenzhe Shi, Andrew Cunningham, and Ferenc Huszár. Lossy image compression with compressive autoencoders, 2017.
- [14] Johannes Ballé, David Minnen, Saurabh Singh, Sung Jin Hwang, and Nick Johnston. Variational image compression with a scale hyperprior. In *6th International Conference on Learning Representations, ICLR 2018, Vancouver, BC, Canada, April 30 - May 3, 2018, Conference Track Proceedings*. OpenReview.net, 2018. URL <https://openreview.net/forum?id=rkcQFMZRb>.
- [15] David Minnen, Johannes Ballé, and George Toderici. Joint autoregressive and hierarchical priors for learned image compression. In *Proceedings of the 32nd International Conference on Neural Information Processing Systems*, pages 10794–10803, 2018.
- [16] Johannes Ballé, Philip A. Chou, David Minnen, Saurabh Singh, Nick Johnston, Eirikur Agustsson, Sung Jin Hwang, and George Toderici. Nonlinear transform coding. *IEEE Trans. on Special Topics in Signal Processing*, 15, 2021. URL <https://arxiv.org/pdf/2007.03034>.
- [17] Sharon Ayzik and Shai Avidan. Deep image compression using decoder side information. In *Computer Vision - ECCV 2020 - 16th European Conference, Glasgow, UK, August 23-28, 2020, Proceedings, Part XVII*, volume 12362, pages 699–714, 2020.
- [18] Nitish Mital, Ezgi Ozyikan, Ali Garjani, and Deniz Gunduz. Neural distributed image compression using common information, 2021.
- [19] Andreas Geiger, Philip Lenz, and Raquel Urtasun. Are we ready for autonomous driving? the kitti vision benchmark suite. In *2012 IEEE conference on computer vision and pattern recognition*, pages 3354–3361. IEEE, 2012.
- [20] Moritz Menze, Christian Heipke, and Andreas Geiger. Joint 3d estimation of vehicles and scene flow. *ISPRS annals of the photogrammetry, remote sensing and spatial information sciences*, 2:427, 2015.
- [21] Ziwei Liu, Ping Luo, Xiaogang Wang, and Xiaoou Tang. Deep learning face attributes in the wild. In *Proceedings of the IEEE international conference on computer vision*, pages 3730–3738, 2015.
- [22] Durk P Kingma and Prafulla Dhariwal. Glow: Generative flow with invertible 1x1 convolutions. In *Neural Information Processing Systems*, pages 10215–10224, 2018.
- [23] Diederik Kingma and Jimmy Ba. Adam: A method for stochastic optimization. *International Conference on Learning Representations*, 12 2014.
- [24] Herbert Robbins and Sutton Monro. A stochastic approximation method. *The annals of mathematical statistics*, pages 400–407, 1951.
- [25] Léon Bottou. Large-scale machine learning with stochastic gradient descent. In *Proceedings of COMPSTAT'2010*, pages 177–186. Springer, 2010.
- [26] John Tsitsiklis, Dimitri Bertsekas, and Michael Athans. Distributed asynchronous deterministic and stochastic gradient optimization algorithms. *IEEE transactions on automatic control*, 31(9):803–812, 1986.
- [27] Yann LeCun, Corinna Cortes, and CJ Burges. Mnist handwritten digit database. *ATT Labs [Online]*. Available: <http://yann.lecun.com/exdb/mnist>, 2, 2010.

[28] Hongyi Wang, Scott Sievert, Shengchao Liu, Zachary Charles, Dimitris Papailiopoulos, and Stephen Wright. Atomo: Communication-efficient learning via atomic sparsification. In *Advances in Neural Information Processing Systems*, pages 9850–9861, 2018.

[29] Anastasia Koloskova, Tao Lin, Sebastian U Stich, and Martin Jaggi. Decentralized deep learning with arbitrary communication compression. *arXiv preprint arXiv:1907.09356*, 2019.

[30] Shaohuai Shi, Xiaowen Chu, Ka Chun Cheung, and Simon See. Understanding top-k sparsification in distributed deep learning. *arXiv preprint arXiv:1911.08772*, 2019.

[31] Sebastian U Stich, Jean-Baptiste Cordonnier, and Martin Jaggi. Sparsified SGD with memory. In *Advances in Neural Information Processing Systems*, pages 4447–4458, 2018.

[32] Dan Alistarh, Demjan Grubic, Jerry Li, Ryota Tomioka, and Milan Vojnovic. QSGD: Communication-efficient SGD via gradient quantization and encoding. In *Advances in Neural Information Processing Systems*, pages 1709–1720, 2017.

[33] Debraj Basu, Deepesh Data, Can Karakus, and Suhas Diggavi. Qsparse-local-SGD: Distributed SGD with quantization, sparsification and local computations. In *Advances in Neural Information Processing Systems*, pages 14668–14679, 2019.

[34] Shaohuai Shi, Qiang Wang, Kaiyong Zhao, Zhenheng Tang, Yuxin Wang, Xiang Huang, and Xiaowen Chu. A distributed synchronous sgd algorithm with global top-k sparsification for low bandwidth networks. In *2019 IEEE 39th International Conference on Distributed Computing Systems (ICDCS)*, pages 2238–2247. IEEE, 2019.

[35] Richard Zhang, Phillip Isola, Alexei A Efros, Eli Shechtman, and Oliver Wang. The unreasonable effectiveness of deep features as a perceptual metric. In *Proceedings of the IEEE conference on computer vision and pattern recognition*, pages 586–595, 2018.

[36] Akash Srivastava, Lazar Valkov, Chris Russell, Michael U Gutmann, and Charles Sutton. Veegan: Reducing mode collapse in gans using implicit variational learning. In *Proceedings of the 31st International Conference on Neural Information Processing Systems*, pages 3310–3320, 2017.

[37] Luke Metz, Ben Poole, David Pfau, and Jascha Sohl-Dickstein. Unrolled generative adversarial networks. *arXiv preprint arXiv:1611.02163*, 2016.

[38] Marton Havasi, Robert Peharz, and José Miguel Hernández-Lobato. Minimal random code learning: Getting bits back from compressed model parameters. In *International Conference on Learning Representations*, 2018.

[39] Jonathan Ho, Xi Chen, Aravind Srinivas, Yan Duan, and Pieter Abbeel. Flow++: Improving flow-based generative models with variational dequantization and architecture design. In *International Conference on Machine Learning*, pages 2722–2730. PMLR, 2019.

A Experiment Details

A.1 VQ-VAE Architecture

For our image compression experiments, we used a convolutional VQ-VAE architecture similar to the one used in [11] with residual connections.

Both the input and the side information to this network have the shape 128×256 (i.e. vertical halves of a full 256×256 image). The encoder scales down input image by a factor of $4 \times$ or $8 \times$ both vertically and horizontally, producing latent variables of shape 32×64 and 16×32 , respectively. Each dimension of the latent variable is allotted different numbers of bits (i.e. codebook bits), which range from 1 to 8 in our experiments. The decoder conversely takes a discrete latent variable and upscales it by a factor of $4 \times$ or $8 \times$ to produce a reconstruction of the original shape.

A detailed specification of the architecture is provided in Figure 7. The notation $\text{Tconv } A \times B (C \rightarrow D)$ represents a 2D (transposed) convolution with kernel size A and stride B with input and output channels C and D , respectively. The boxes “Residual Block ($A \rightarrow B$)” represent a two-layer residual network. We used GELU (Gaussian Error Linear Unit) activation for all layers except for the very last convolution of the decoder, for which we used sigmoid. The exact number of channels may differ for different rate-distortion points, and we refer the reader to the supplementary code submission for full details.

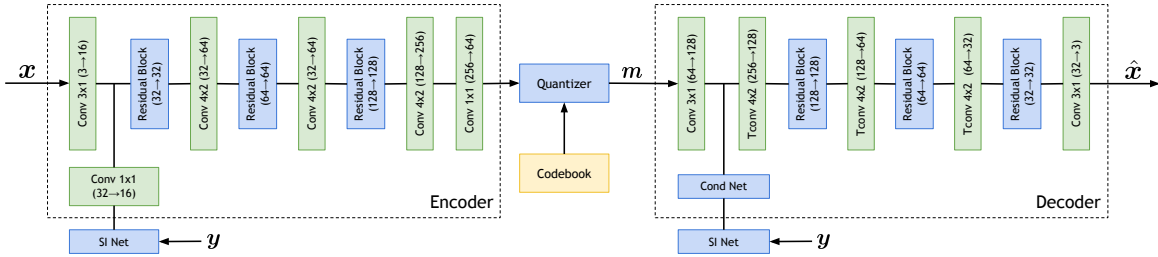


Figure 7: Conditional VQ-VAE architecture used for the image compression experiments.

We used a small network (denoted “SI Net”) shared by the encoder and decoder to preprocess the side information. Whenever the encoder or decoder does not receive side information (for distributed and separate VQ-VAEs), we simply replace the output of SI Net with a zero tensor of the same shape.

We note that all three VQ-VAE variants have the same architecture and number of parameters for the autoencoder portion (the portion that the horizontal line goes through in Figure 7). Thus there is no architectural advantage among the VQ-VAE variants.

A.2 Specifying Target Rate

The shape and the number of codebook bits determine the total rate. This is different from neural compression models that use a regular VAE, which control rate-distortion by reweighting the training objective (ELBO). As mentioned in section 2.2, the fact that we have a hard constraint on the rate is useful when working with a hard communication limit.

There are several ways to achieve a desired target rate. For example, an $8 \times$ downscaling encoder with 4 codebook bits produces compressed message of size $16 \times 32 \times 4 = 2048$ bits. The same rate can be achieved using a $4 \times$ downscaling encoder with 1 codebook bit: $32 \times 64 \times 1 = 2048$ bits. This flexibility is what allows us to have a fairly granular control over the target rate, at the cost of hyperparameter choices.

Hyperparameters for KITTI Stereo Experiment. Due to the above choices, we use differently

sized networks for each rate-distortion curve for our stereo image compression experiments. While the model definition is included in the code, we include the relevant hyperparameter information in table 3 below.

Table 3: Different models and their associated hyperparameters for the stereo image compression experiment. Each row represents a single rate-distortion point in fig. 2a.

Downscaling Factor	Codebook Size (bits)	Rate (bpp)	Distortion (PSNR)	Parameter count
8×	1	0.0156	20.77	3,954,853
8×	2	0.0312	21.884	3,955,111
8×	3	0.469	22.658	6,250,747
8×	8	0.125	24.687	4,037,827
4×	3	0.1875	25.642	6,276,619
4×	4	0.2500	26.582	6,277,651
4×	6	0.3750	27.531	6,283,843

Hyperparameters for CelebA-HQ Experiment. For this experiment, we used the single 8× downscaling encoder with codebook bits {1,2,3,4}, resulting in the total rates of {512, 1024, 1536, 2048}.

Distributed optimization. For gradient compression VQ-VAEs, we followed the same architecture as the image compression experiments, but replaced all convolutional layers with fully-connected layers. Full specification of the network is included in the code submission.

A.3 Stereo Image Dataset

For our stereo image compression experiment, we follow the setup of [18]. First, we construct training/test datasets using the files specified in the official repository for [17] (https://github.com/ayziksha/DSIN/tree/master/src/data_paths). Then we apply the same preprocessing steps of [18], where we first take the center crop of size 370×740 , then resizing it to 128×256 using PyTorch transformations. This results in the training split containing 1576 pairs of stereo images and test split containing 790 pairs.

A.4 Training Details

For stereo image compression experiments, we trained our models for up to 1000 epochs on a DGX machine. Some training runs were early stopped because the validation performance started to plateau. For CelebA-HQ experiments, we trained the VQ-VAEs for a total of 20 epochs distributed over two Nvidia GTX 2080 GPUs. For gradient compression experiments, we trained the fully-connected VQ-VAEs for 500 epochs on a single GPU.

In all cases, we evaluated validation loss after each epoch and observed no overfitting. This leads us to believe that it may be possible to further improve the performance of our method by training a larger network, which we leave for future work.

A.5 NDIC Training Details

For the CelebA-HQ compression experiment, we trained NDIC [18] using the official code released by the authors. We used the “Balle18” [14] backbone and trained the model for 10 epochs (≈ 300 K examples). For evaluation, we used the model checkpoint with the best validation set performance. While Mital et al. [18] report training with a batch size of 1 for 500K steps, we chose to use a batch size of 20. This was done for several reasons. First, using a batch size of 1 is very inefficient as we do not benefit from parallelism of GPU. It also leads to high variance in the gradient, often leading to slower

convergence. In our training, the loss plateaued well before reaching 300K total examples. We also used MSE instead of MS-SSIM as the objective, since our models were also trained using MSE loss. This ensures a fair comparison in both training as well as evaluation, as we report PSNR (which is equivalent to MSE). The rest of the model hyperparameters were not modified.